Cyclometalated Platinum(II) Complex with Strong and Broadband Nonlinear Optical Response

Pin Shao, Yunjing Li, and Wenfang Sun*

Department of Chemistry and Molecular Biology, North Dakota State University, Fargo, North Dakota 58105

Received: November 5, 2007

A cyclometalated platinum(II) 4,6-diphenyl-2,2′-bipyridyl pentynyl complex (**1**) has been synthesized and structurally characterized. Its photophysical and third-order nonlinear optical properties have been systematically investigated. This complex exhibits a metal-to-ligand charge-transfer (^{1}MLCT) absorption band between 400 and 500 nm and a ^{3}MLCT emission band at ∼591 nm at room temperature with a lifetime of ∼100 ns. At 77 K, the emission band blue shifts. Both UV−vis absorption and emission spectra show solvent dependence. Low-polarity solvents cause a bathochromic shift of the absorption and emission bands. This complex also exhibits a broad and strong transient absorption from the near-UV to the near-IR spectral region, with a triplet absorption coefficient of 4933 $L \cdot mol^{-1} \cdot cm^{-1}$ at 585 nm and a quantum yield of 0.51 for the formation of the triplet excited state. Nonlinear transmission and Z-scan techniques were employed to characterize the third-order nonlinearities of this complex. A strong and broadband reverse saturable absorption was observed for nanosecond and picosecond laser pulses due to the reduced ground-state absorption in the visible spectral range. It also exhibits a self-defocusing effect at 532 nm for nanosecond laser pulses. The excited-state absorption cross section deduced from the open-aperture Z-scan increases at longer wavelengths, with an exceptionally large ratio of excited-state absorption to ground-state absorption of 160 at 570 nm for picosecond laser pulses.

Introduction

Square-planar platinum(II) complexes have attracted great interest in recent years due to their potential applications as photocatalysts[1] and in a variety of photonic devices, such as light-emitting diodes,[2] photovoltaic cells,[3] and chemosensors.[4] In these complexes, platinum(II) bonded with a large conjugated ligand(s) often leads to interaction between the metal center and the organic molecule framework. As a result, the electron delocalization of the complexes would be extended, and the molecules could possess a large third-order nonlinear optical response. In addition, the heavy-metal effect of the platinum(II) ion could enhance the intersystem crossing (ISC) rate to the triplet excited states and thus favors the triplet excited-state-based reverse saturable absorption (RSA) and nonlinear transmission process.[5]

It is well-known that in order to increase the RSA, the materials are required to possess a large ratio of excited-state absorption to ground-state absorption cross sections, a high quantum yield of excited-state formation, and/or a long-lived excited state. Presently, molecules exhibiting a strong RSA effect usually possess large rigid conjugated frameworks, such as porphyrins,[6] phthalocyanines,[7] and fullerenes.[8] These rigid compounds usually have poor solubility and dark colors, and thus, their practical applications are limited. Recently, some platinum(II) alkynyl complexes were reported to show large reverse saturable absorption and broad spectral and temporal nonlinear transmission behavior.[9] However, some of these complexes are not quite stable upon exposure to UV light and laser beams.[9d] This motivates us to investigate the more photostable terdentate platinum(II) complexes. Our studies have revealed that a variety of mononuclear and multinuclear platinum(II) terpyridyl and 4,6-diphenyl-2,2′-bipyridyl complexes exhibit relatively long triplet excited-state lifetimes, broad and moderately strong excited-state absorption, and reasonably high quantum yields to form the triplet excited state.[10] All of these merits lead to a strong reverse saturable absorption for nanosecond laser pulses at 532 nm.[10] Most importantly, we have discovered that the excited-state characteristics, such as energy level, lifetime, and excited-state absorption, are influenced drastically by the nature of the terdentate ligand, the auxiliary substituents on the terdentate and the acetylide ligands, as well as the bridging ligand in the case of multinuclear complexes. Among all of the complexes synthesized and investigated in our group, the 4,6-diphenyl-2,2′-bipyridyl (dphbpy) and pentynyl ligands were found to give rise to the strongest RSA in their corresponding series of complexes. To figure out whether a synergistic enhancement occurs when the optimized ligands are combined, a new platinum(II) complex **1** containing the 4,6-diphenyl-2,2′-bipyridyl and pentynyl ligands (Figure 1) was synthesized, and its photophysical and nonlinear optical properties have been systematically investigated. Its photophysical and RSA behaviors have been compared to those of the platinum(II) 6-phenyl-4-tolyl-2,2′-bipyridyl phenylacetylide complex (**2**)[10a] and the platinum(II) terpyridyl pentynyl complex (**3**).[10c] As expected, this new complex exhibits not only stronger RSA to nanosecond laser pulses at 532 nm but also a broad spectral nonlinear optical response to picosecond laser pulses.

Experimental Section

Synthesis. The precursor complex 4,6-diphenyl-2,2′-bipyridine platinum chloride (dphbpyPtCl) was synthesized according to the reported procedures.[11] All of the starting chemicals were

* To whom correspondence should be addressed. E-mail: Wenfang.Sun@ndsu.edu.

10.1021/jp710616z CCC: $40.75
Published on Web 01/15/2008

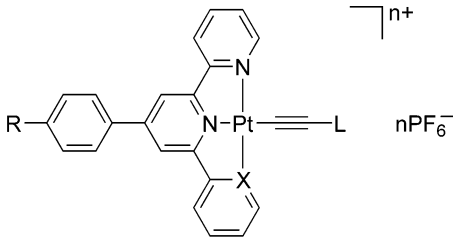

R =	X =	L =	n =	
H	C	C_3H_7	0	**1**
CH_3	C	C_6H_5	0	**2**
CH_3	N	C_3H_7	1	**3**

Figure 1. Chemical structures of complexes **1**−**3**.

purchased from Alfa Aesar. Solvents were used as received unless otherwise stated.

^{1}H NMR spectra were measured on a Varian 400 MHz VNMR spectrometer. ESI-HRMS analyses were conducted on a Bruker Daltonics BioTOF III mass spectrometer. Elemental analyses were performed on a Perkin-Elmer 2400 Series II CHNS/O analyzer.

(1) A mixture of 25 mg of KOH in 3 mL of DMF was purged with argon for 30 min; then, 0.1 mL of pentyne was added, the mixture was stirred for 30 min, and 78 mg of dphbpyPtCl and 5 mg of CuI were added. After the mixture was stirred under argon at room temperature for 36 h, 50 mL of ether was added. The crude product was collected by filtration, purified by passing through a short aluminum oxide column three times, and recrystallized by diffusing ether into CH_2Cl_2; yield: 17%. ^{1}H NMR ($CDCl_3$) δ: 9.15 (s, 1H), 7.90−7.97 (m, 3H), 7.67−7.68 (m, 3H), 7.58 (s, 1H), 7.47−7.51 (m, 4H), 7.50 (d, $J = 7.6$ Hz, 1H), 7.14 (t, $J = 7.2$ Hz, 1H), 7.01 (t, $J = 7.2$ Hz, 1H), 2.65 (t, $J = 7.2$ Hz, 2H), 1.70 (hex, $J = 7.2$ Hz, 2H), 1.11 (t, $J = 7.2$ Hz, 3H) ppm. ESI-MS: *m*/*z* calcd for $[C_{27}H_{23}N_2Pt^{195}]^+$, 570.4575; found, 570.2392 (100%). Anal. Calcd for $C_{27}H_{22}N_2Pt$: C, 56.94; H, 3.89; N, 4.92. Found: C, 57.44; H, 3.51; N, 5.31.

Crystal Structure Determination. A crystal with dimensions of 0.3 × 0.2 × 0.2 mm was mounted on a glass fiber and coated with super glue. The crystal was transferred to a Bruker CCD diffractometer with Mo Kα radiation ($\lambda = 0.71073$ Å). The frames were collected at ambient temperature with a scan width of 0.3° in ω and integrated with the Bruker SAINT software package using the narrow-frame integration algorithm. The unit cell was determined and refined by least-squares upon the refinement of *XYZ*-centroids of reflections above 20σ(*I*). The data were corrected for absorption using the SADABS program. The structures were refined on F^2 using the WinGx software package.[12] Post-refinement of the unit cell gave $a = 16.2361(6)$ Å, $b = 9.5110(4)$ Å, $c = 17.9203(6)$ Å, $\alpha = 90$, $\beta = 114.692(2)$, $\gamma = 90$, and $V = 2514.26(16)$ Å.^{3} The compound has monoclinic space group *P*21/*c*.

The structure was solved by the direct method. All of the non-hydrogen atoms were refined with anisotropic displacement coefficients. Hydrogen atoms were located and refined isotropically using SHELXL97.[13] The weighting scheme employed was $w = 1/[\sigma^2(F_o^2) + (0.308P)^2 + 46.6743P]$ where $P = (F_o^2 + 2F_c^2)/3$. The refinement converged to $R_1 = 0.0636$, $wR_2 = 0.1238$ for reflections with $1 > 2\sigma(I)$, $R_1 = 0.1195$, $wR_2 = 0.1583$ for all data ($R_1 = \Sigma(||F_o| - |F_c||)/\Sigma|F_o|$, $wR_2 = [\Sigma(w(F_o^2 - F_c^2)^2)/(F_o^2)^2]^{1/2}$, and S = goodness-of-fit on $F^2 = [\Sigma(w(F_o^2 - F_c^2)^2/(n - p)]^{1/2}$, where n is the number of reflections and p is the number of parameters refined.) Crystallographic and structural refinement data are listed in Table 1.

TABLE 1: Crystallographic and Structural Refinement Data for 1

empirical formula	$C_{28}H_{24}Cl_2N_2Pt$
FW	654.48
crystal system	monoclinic
space group	*P*21/*c*
a/Å	16.2361(6)
b/Å	9.5110(4)
c/Å	17.9203(6)
α/deg	90
β/deg	114.692(2)
γ/deg	90
V/Å^3	2514.26(16)
Z	4
ρ_{calcd}/g·cm^{-3}	1.729
μ/cm^{-1}	5.812
F(000)	1272
T/K	293(2)
wavelength/ Å	0.71073
data collection range/deg	2.30-25.24
index ranges	$-19 \le h \le 19, -11 \le k \le 11, -21 \le l \le 21$
reflections collected/unique	21020/4363 [*R*(int) = 0.1099]
final [$I > 2\sigma(I)$][a]	$R_1 = 0.0636$, $wR_2 = 0.1238$
R indices (all data)[a]	$R_1 = 0.1195$, $wR_2 = 0.1583$

[a] $R_1 = \Sigma(||F_o| - |F_c||)/\Sigma|F_o|$; $wR_2 = [\Sigma(w(F_o^2 - F_c^2)^2)/\Sigma(F_o^2)^2]^{1/2}$

Photophysical Measurements. The UV−vis absorption spectra were measured using an Agilent 8453 spectrophotometer in a 1 cm quartz cuvette in CH_3CN solution. The steady-state fluorescence spectra were obtained on a SPEX fluorolog-3 fluorometer/phosphorometer in CH_3CN solution. The excited-state lifetimes, the triplet excited-state quantum yields, and the triplet transient difference absorption spectra were measured in CH_3CN solutions on an Edinburgh LP920 laser flash photolysis spectrometer. The third harmonic output (355 nm) of a Nd:YAG laser (Quantel Brilliant, pulse width ~ 4.1 ns, repetition rate 10 Hz) was used as the excitation source. Each sample was purged with Ar for 30 min before measurement.

The triplet excited-state molar extinction coefficient and triplet quantum yield were determined by the partial saturation method.[14] The optical density at 585 nm was monitored when the excitation energy at 355 nm was gradually increased. Saturation was observed when the excitation energy was higher than 10 mJ. The following equation was then used to fit the experimental data to obtain the ϵ_T and Φ_T[14]

$$\Delta OD = a(1 - \exp(-bI_p)) \quad (1)$$

where ΔOD is the optical density at 585 nm, I_p is the pump intensity in Einstein·cm^{-2}, $a = (\epsilon_T - \epsilon_0)dl$, and $b = 2303\,\epsilon_0^{ex}\Phi_T/A$. ϵ_T and ϵ_0 are the absorption coefficients of the excited state and the ground state at 585 nm, ϵ_0^{ex} is the ground-state absorption coefficient at the excitation wavelength of 355 nm, d is the concentration of the sample (mol·L^{-1}), l is the thickness of the sample, and A is the area of the sample irradiated by the excitation beam.

Nonlinear Transmission Measurements. The experimental setup was similar to what had been described previously,[10d] with a 20 cm lens used to focus the beam to the sample cuvette. The thickness of the cuvette is 2 mm.

Z-Scan Measurements. The experimental setup is shown in Figure 2. The light sources were a Quantel Brilliant Nd:YAG laser with a pulse width of 4.1 ns and a repetition rate of 10 Hz for nanosecond Z-scan measurements and an EKSPLA PG401 Optical Parametric Generator (OPG) pumped by an EKSPLA PL2143A passively mode-locked, Q-switched Nd:YAG laser with a pulse width of 27 ps and a repetition rate of 10 Hz for picosecond Z-scan measurements. The energy from the laser

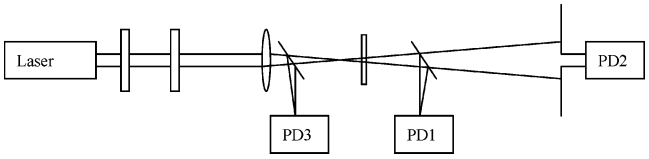

Figure 2. The experimental setup for Z-scan measurements.

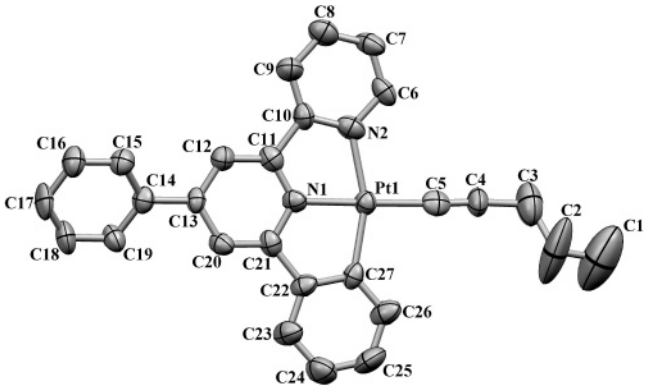

Figure 3. ORTEP diagram of complex **1** with 50% ellipsoid probability. Hydrogen atoms and solvent molecules have been omitted for clarity.

was attenuated through a combination of a half-wave plate and a polarizing cube beam splitter. For the nanosecond Z-scan, the laser beam was focused by a 20 cm focal length plano-convex lens to a beam waist of 20.5 μm at the focal point, which gives rise to a Rayleigh length ($z_0 = \pi\omega_0^2/\lambda$, where ω_0 is the radius at the beam waist) of 2.48 mm. The sample solution was placed in a 1 mm thick quartz cuvette. For the picosecond Z-scan, the lens used was a 15 cm plano-convex lens with a beam waist of 33.0 μm at the focal point, which corresponds to a Rayleigh length of 6.42 mm. Thus, a 2 mm cuvette was used for the picosecond Z-scan measurements. The cuvette was placed on a motorized translation stage and was moved back and forth through the focal point. The movements of the translation stage and the data acquisition were controlled by a computer. A wedged beam splitter was placed ~44 cm after the focal plane of the lens in order to measure the open aperture and closed aperture Z-scan simultaneously. An iris aperture was used in front of the detector PD2 for the closed aperture Z-scan measurement. The photodetectors used were Molectron J4-09 joulmeters.

Results and Discussion

Crystal Structure. A single crystal of **1** was obtained by slow diffusion of ether into its dilute CH_2Cl_2 solution. The single-crystal X-ray diffraction result confirms a distorted square-planar geometry around the Pt center, similar to the platinum acetylide complexes reported in the literature.[1a] The bond length of Pt(1)−C(5) is 1.982(16) Å, which is comparable to the length of reported platinum acetylide complexes.[1a,2a,3e] The phenyl ring is almost coplanar with the C^N^N plane with a torsion angle of 27.17°. The two neighboring molecules are stacked parallel in a head-to-tail fashion (Figure 4), with a $\pi-\pi$ contact of ~3.505 Å. The shortest distance between two neighboring Pt atoms is 7.122 Å; therefore, no intermolecular Pt···Pt interactions are possible. The selected bond lengths and bond angles are listed in Table 2.

UV−Vis Absorption. The electronic absorption spectrum of **1** in acetonitrile solution is shown in Figure 5. It features a broad low-energy band in the range of 400−500 nm ($\epsilon \approx 5.8 \times 10^3$ L·mol^{-1}·cm^{-1}), which is ascribed to the metal-to-ligand charge-transfer (^{1}MLCT) transition with reference to similar cyclometalated platinum(II) alkynyl complexes reported in the literature.[15] The high-energy absorption bands at 280−390 nm are assigned to the $^1\pi,\pi^*$ transition within the dphbpy ligand. The UV−vis absorption of **1** follows Beer's law in the concentration range of 2.1×10^{-6} to 5.0×10^{-4} mol/L, indicating that no aggregation occurs at this concentration range. Temperature also shows no effect on the UV−vis spectrum from 0 to 48 °C. This suggests that no conformational change or intermolecular interaction occurs within this temperature range. In contrast, the polarity of the solvent influences the UV−vis spectrum of **1**. As shown in Figure 6, low-polarity solvents, such as toluene and THF, cause a significant red shift of the whole spectrum; especially the ^{1}MLCT band exhibits a 40 nm bathochromic shift in comparison to that in acetonitrile. This indicates that the ground state of **1** is more polar than that of the excited state, which has been observed in many other square-planar platinum(II) complexes.[10b,11]

TABLE 2: Selected Bond Lengths (Å) and Bond Angels (deg) for 1

Pt(1)−C(5)	1.982(16)	Pt(1)−N(1)	1.986(10)
Pt(1)−C(27)	2.060(13)	Pt(1)−N(2)	2.109(12)
C(4)−C(5)	1.176(19)	C(5)−Pt(1)−N(1)	179.1(5)
C(5)−Pt(1)−C(27)	99.7(5)	N(1)−Pt(1)−C(27)	81.2(5)
C(5)−Pt(1)−N(2)	101.0(5)	N(1)−Pt(1)−N(2)	78.2(4)
C(27)−Pt(1)−N(2)	159.4(5)	C(5)−C(4)−C(3)	176.2(19)

It is also interesting to note that the UV−vis spectrum of **1** is more similar to that of the complex **2**, which contains the same C^N^N terdentate ligand but has a phenylacetylide ligand instead of the pentynyl ligand. This suggests that it is the terdentate ligand rather than the auxiliary ligand that determines the feature of the UV−vis absorption spectrum.

Emission. Complex **1** is emissive at room temperature and 77 K in a variety of solvents. Figure 7 displays its emission spectra in acetonitrile solution at room temperature and acetonitrile glassy solution at 77 K. When excited at either 367 nm or 432 nm, **1** exhibits only one short-lived (102 ns) emission band at ~591 nm at room temperature, which is ascribed to the ^{3}MLCT excited state. In contrast, excitation at 332 nm results in an additional high-energy emission band at ~397 nm along with the ^{3}MLCT band at 591 nm (see Supporting Information Figure S4). This high-energy band is consistent with the emission band from the dphbpy ligand and, therefore, is ascribed to the $^1\pi,\pi^*$ state of the ligand. Additional support of the different origins of these two emission bands arises from the excitation spectra monitored at 397 and 591 nm, respectively. As shown in Figure 8, the excitation spectrum corresponding to the 397 nm emission band appears at 314 nm, while the excitation spectrum monitored at 591 nm gives rise to a structured feature with band maxima at 339, 372, 439, 454, and 475 nm. In addition, the 397 nm emission band and the 591 nm band exhibit quite different lifetimes. As shown in Table 3, the lifetime of the 591 nm emission band is 102 ns in acetonitrile, while the lifetime of the 397 nm emission band is too short to be measured by our instrument, whose resolution is approximately 5 ns. All of these clearly indicate the different parentages of these two emission bands.

When the concentration of the solution increases from 1.9×10^{-5} to 5.0×10^{-4} mol/L, the intensity of the emission band at ~397 nm decreases, while the intensity of the band at 591 nm keeps increasing. The decrease of the emission intensity of the 397 nm band is presumably attributed to self-quenching that is commonly seen in many other organometallic complexes.[16] However, because of the considerable ground-state absorption at 397 nm, the inner filter effect may also play a role. Due to

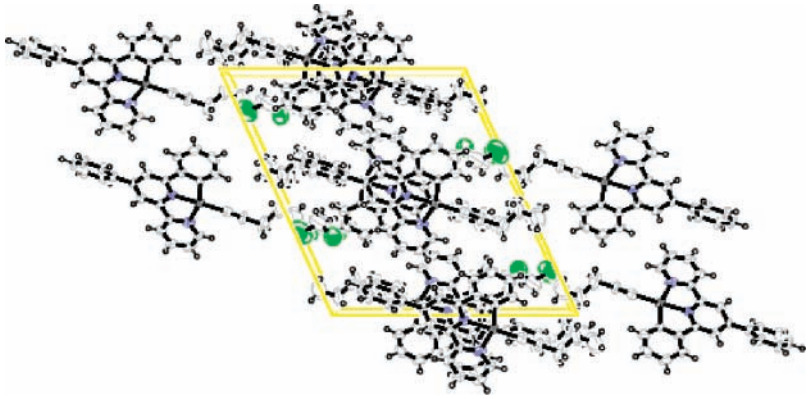

Figure 4. Packing diagram of **1** with 50% ellipsoid probability. View normal to (010).

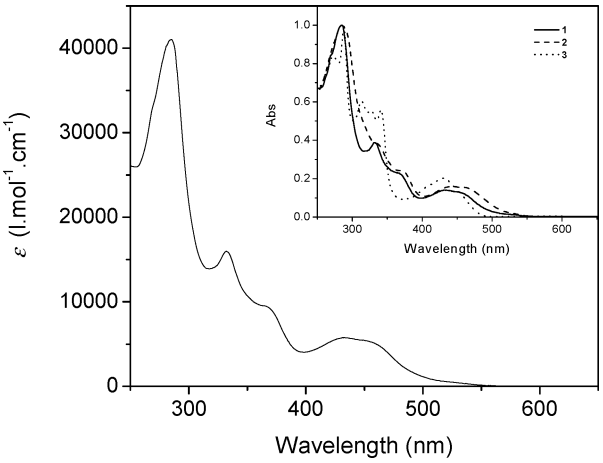

Figure 5. UV−vis absorption spectrum of **1** in acetonitrile. The inset shows the comparison of the normalized absorption spectra of **1**−**3** in acetonitrile.

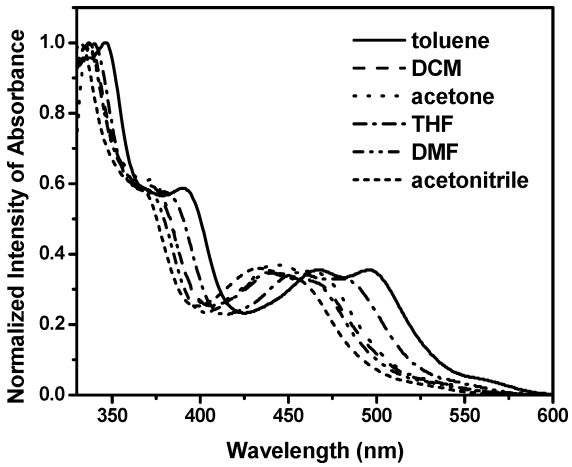

Figure 6. UV−vis absorption spectrum of a 3.5×10^{-5} mol/L solution of **1** in different solvents measured in a 1 cm cuvette.

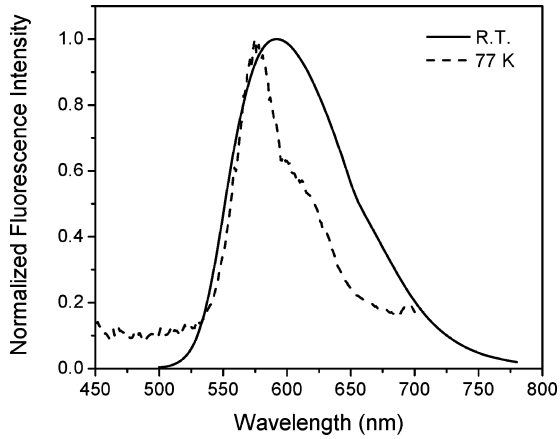

Figure 7. Emission spectrum of **1** in acetonitrile at room temperature and 77 K. The solution concentration is 3.4×10^{-5} mol/L; $\lambda_{ex} = 432$ nm.

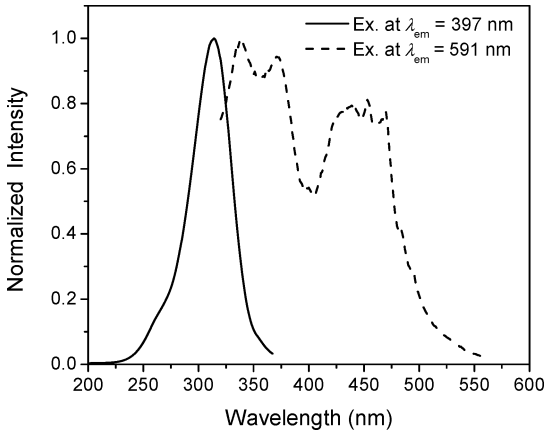

Figure 8. Excitation spectra of **1** in acetonitrile at room temperature monitored at different emission bands. The solution concentration is 1.9×10^{-5} mol/L.

the limited resolution of our spectrometer, the lifetime of the 397 nm emission band could not be measured. Therefore, the relative contribution from the self-quenching and the inner filter effect cannot be identified.

Variation of the temperature from 0 to 48 °C reveals that only the intensity of the emission decreases at elevated temperatures due to the increased nonradiative decay at high temperatures. The emission energy was not influenced by the temperature variation.

The solvent-dependent emission study (see Table 3 and Supporting Information) demonstrates that the emission energy decreases in low-polarity solvents, such as toluene and THF, which is consistent with the observation from the UV−vis absorption measurement. This indicates that both the singlet and triplet MLCT states are less polar than the ground state for **1**.

Emission measured in acetonitrile glassy solution at 77 K reveals that the emission band becomes narrower and blue shifted in comparison to that measured at room temperature. This could be attributed to the rigidochromic effect that is commonly observed in metal diimine and terpyridyl complexes.[17] The emission at 77 K also exhibits concentration dependence. However, unlike the phenomenon observed at room temperature, with increased concentration, the emission band

TABLE 3: Solvent-Dependent Emission and Transient Absorption Results for 1 at Room Temperature at a Concentration of 3.4×10^{-5} mol/L

solvent	λ_{em}/nm (τ/ns)	Φ_{em}[a]	λ_{TA}/nm (τ/ns)
toluene	600 (173)	0.031	420 (174); 590 (167)
THF	605 (35)	0.003	405 (29); 585 (34)
acetone	600 (145)	0.025	410 (149); 570 (126)
DMF	590 (49)	0.003	575 (51)
acetonitrile	589 (102)	0.025	385 (86); 585 (87)

[a] Quantum yield of emission relative to $[Ru(bpy)_3]Cl_2$ ($\Phi_{em} = 0.042$),[19] $\lambda_{ex} = 436$ nm.

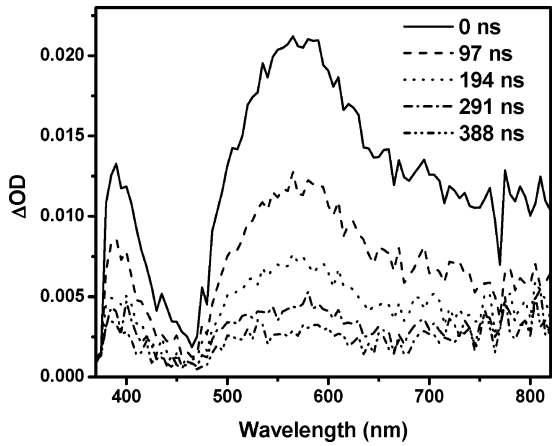

Figure 9. The time-resolved triplet transient difference absorption of **1** in CH_3CN at room temperature at a concentration of 5.6×10^{-5} mol/L; $\lambda_{ex} = 355$ nm. The time shown in the figure is the time delay after laser excitation.

at 77 K gradually red shifts from 532 nm for a 2.1×10^{-5} mol/L glassy solution to 566 nm for a 3.4×10^{-4} mol/L glassy solution (see Supporting Information). This red shift could be tentatively attributed to an increased degree of aggregation at higher solution concentrations. A similar phenomenon has been reported by Che and co-workers for a trinuclear planitum(II) 6-phenyl-2,2′-bipyridyl complex at 298 K.[18] The presence of ground-state aggregates at 77 K in glassy solutions but not at room temperature in fluid solutions for **1** at the similar concentration indicates that the association constant for the aggregation process could be too small to be observed at room temperature. This has been confirmed by the UV−vis absorption spectra measurement at different concentrations. No bathochromic shift or peak broadening has been observed for **1** from the concentration of 2.1×10^{-6} to 5.0×10^{-4} mol/L, as described earlier in the UV−Vis Absorption section. Unfortunately, the measurement of the concentration-dependent electronic absorption spectra at 77 K could not be carried out due to our current instrument limitation. The attribution to an inner-filter effect could be excluded because of the negligible ground-state absorption above 500 nm.

Triplet Transient Difference Absorption. The time-resolved triplet transient difference absorption spectrum of **1** in acetonitrile is displayed in Figure 9. It exhibits two positive bands from 370 to 820 nm, one appearing at ~385 nm and another at ~585 nm. Most importantly, the whole spectrum is positive, indicating that from near-UV to near-IR, the excited-state absorption is stronger than that of the ground state, which is broader than those of the corresponding terpyridyl complex **3**[10c] and diphenylbipyridyl phenylacetylide complex **2**.[10a] Therefore, RSA could occur in a broad spectral range. Similar to what has been observed from the UV−vis absorption spectra, the shape of the triplet transient difference absorption spectrum of **1** is more similar to that of **2**. This confirms that the terdentate ligand rather than the acetylide ligand determines the shape of the absorption spectra, in both the ground state and excited state. In addition, both bands exhibit monoexponential decay, with a short lifetime of 86 ns at 385 nm and 87 ns at 585 nm. Compared to the similar short lifetime of the ^{3}MLCT emission (102 ns), the transient absorption could also arise from the same excited state that emits or a state that is in equilibrium with the emitting state. Therefore, the transient absorption could be attributed to the ^{3}MLCT state.

Using the partial saturation method,[14] the optical density at 585 nm was monitored at excitation energies between 0.5 and 35 mJ. Saturation was observed when the excitation energy was higher than 10 mJ (see Supporting Information). Through the curve fitting, the excited-state absorption coefficient at 585 nm was found to be 4933 $L \cdot mol^{-1} \cdot cm^{-1}$, and the triplet quantum yield was determined to be 0.51. This triplet quantum yield is comparable to those of the platinum(II) terpyridyl arylacetylide complexes previously reported by our group.[10b]

Reverse Saturable Absorption. The photophysical studies have revealed that **1** exhibits a positive transient absorption from near-UV to near-IR, and the triplet lifetime is about 100 ns in CH_3CN solution. It also exhibits a high yield of triplet excited-state formation. Therefore, reverse saturable absorption should occur in this spectral range. To demonstrate this, nonlinear transmission measurements were conducted at 532 nm using both nanosecond and picosecond laser pulses. Different pulse width lasers were used because, in general, the nanosecond nonlinear transmission experiment measures the nonlinear absorption mainly arising from the triplet excited state, while the picosecond measurement determines the contribution mainly from the singlet excited state. Figure 10 shows the nonlinear transmission results of **1** for both nanosecond and picosecond laser pulses. With a linear transmission of 90% in a 2 mm thick quartz cell, the acetonitrile solution of **1** exhibits a significant transmission drop with increased incident fluence, which clearly suggests a reverse saturable absorption (RSA). For nanosecond laser pulses, the threshold for RSA, defined as the incident fluence at which the transmittance decreases to 70% of the linear transmittance, is found to be 40 mJ/cm^2 for **1**. This value is much lower than the 52 mJ/cm^2 threshold for **2** at the same linear transmittance and the same experimental conditions. For **3**, the transmission did not drop to 70% of the linear transmission even at the highest incident fluence; therefore, the RSA threshold was not able to be determined. When the incident fluence was increased to 0.12 J/cm^2, the transmittance decreased to 44% for **1**, 51% for **2**, and 68% for **3**. The strong RSA of **1** suggests that **1** possesses a much larger ratio of the excited-state absorption to the ground-state absorption cross section than those of **2** and **3,** which will be confirmed from the fitting of the open-aperture Z-scan results that will be described in the following section.

In addition, **1** exhibits RSA for picosecond laser pulses. For a solution with 75% linear transmission in a 2 mm cell, the transmission of the solution decreases to 45% at an incident fluence of 0.2 J/cm^2. Comparing the RSA of **1** for picosecond and nanosecond laser pulses, it is obvious that the RSA is stronger for the nanosecond laser pulses than that for picosecond laser pulses. This phenomenon is likely to be due to the differences in the singlet and the triplet excited states. As mentioned earlier, RSA for nanosecond laser pulses generally mainly arises from the triplet excited state, while the RSA for picosecond laser pulses usually is dominated by the singlet excited state when the intersystem crossing time is longer than the laser pulse width. The stronger RSA for nanosecond than

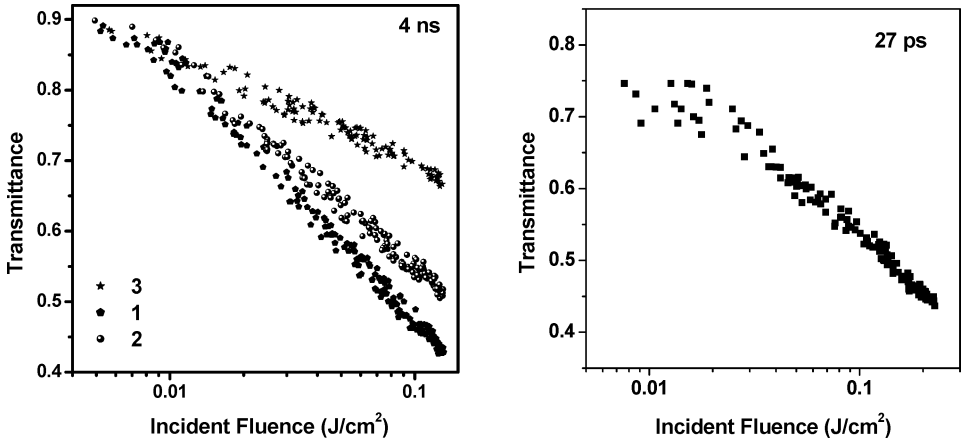

Figure 10. Nonlinear transmission curves of **1** for 4.1 ns and 27 ps laser pulses at 532 nm in a 2 mm cell. The linear transmission was adjusted to 90% for nanosecond measurements and 75% for picosecond measurements. The concentration used for the nanosecond measurement was 5.5×10^{-4} mol/L for **1**, 2.4×10^{-4} mol/L for **2**, and 1.7×10^{-3} mol/L for **3**. The concentration of **1** used for the picosecond measurement was 1.5×10^{-3} mol/L. All samples were dissolved in CH_3CN.

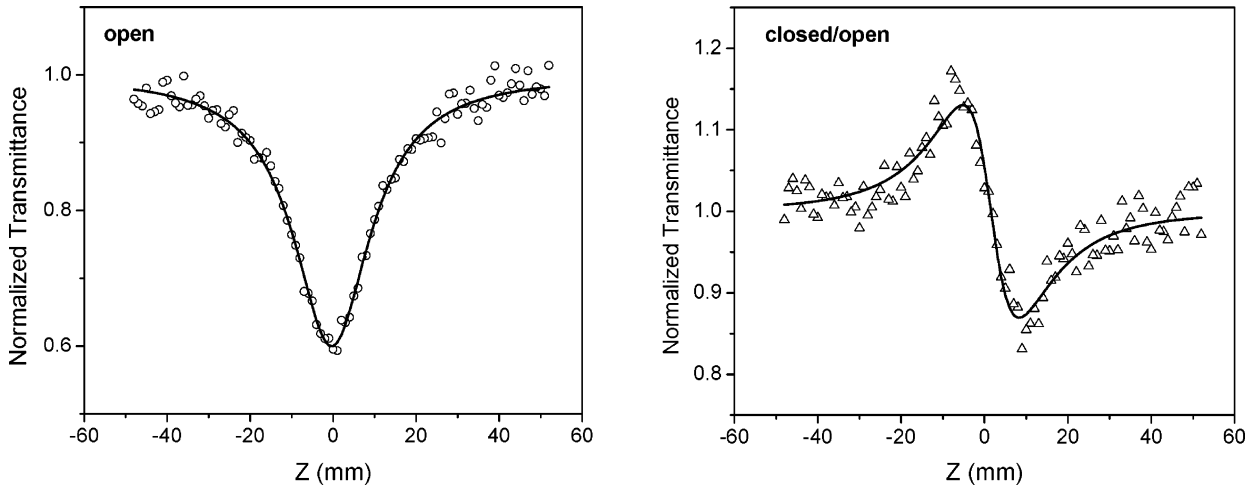

Figure 11. Open- and closed-aperture Z-scan of **1** using 4.1 ns laser pulses at 532 nm in a 1 mm cell. The incident energy of the laser beam is 7.4 μJ, and the concentration used is 1.9×10^{-3} mol/L.

for picosecond laser pulses suggests that the triplet excited-state absorption cross section is larger than that of the singlet excited state, which is consistent with the Z-scan result discussed in the following section. Nevertheless, **1** shows strong RSA not only for nanosecond but also for picosecond laser pulses.

Z-Scan Measurements. It is well-known that third-order nonlinear susceptibility is a complex number, with the real part related to nonlinear refraction and the imaginary part related to nonlinear absorption. The nonlinear transmission discussed in the previous section only measures the contribution from the nonlinear absorption. To figure out whether **1** exhibits nonlinear refraction and the contribution from nonlinear absorption and nonlinear refraction, a Z-scan[20] experiment was conducted.

Z-scan[20] is a simple technique that is used to measure the on-axis phase change ($\Delta\Phi_0$) of a laser beam when it propagates through nonlinear media. It gives rise to both the sign and the magnitude of this phase change. The magnitude of $\Delta\Phi_0$ is related to the nonlinear refractive index (n_2) of a third-order nonlinear optical material by the following equation[20]

$$n_2(m^2/W) = \frac{\Delta\Phi_0\lambda}{2\pi L_{\text{eff}} I_0} \tag{2}$$

where $L_{\text{eff}} = (1 - e^{\alpha L})/\alpha$ is the effective beam path, with α as the linear absorption coefficient, and I_0 is the on-axis ($r = 0$), peak ($t = 0$) irradiance with the nonlinear media at the focal plane ($Z = 0$). For a Gaussian spatial and temporal distribution, $I_0 = 4\sqrt{\ln 2}E_{\text{total}}/\sqrt{\pi^3}\omega_0^2\tau$, where E_{total} is the incident energy on the sample after the reflection from the front surface of the cell is taken into account, ω_0 is the radius of the beam waist at the focal point, and τ is the pulse width (full width at half-maximum). For a Gaussian beam Z-scan, $\Delta\Phi_0$ can be obtained from the fitting of the normalized nonlinear refraction curve (closed aperture/open aperture) using the following equation[20]

$$T(z,\Delta\Phi) = 1 - \frac{4\Delta\Phi_0(z/z_0)}{[(z/z_0)^2 + 1][(z/z_0)^2 + 9]} \tag{3}$$

where T is the normalized transmission, z is the distance of the sample relative to the focal plane, and z_0 is the Rayleigh length.

The n_2 is related to the real part of $\chi^{(3)}$ by[21]

$$\text{Re}\chi^{(3)}(\text{esu}) = \frac{cn_0^2}{720\pi^2} n_2(m^2/W) \tag{4}$$

As shown in Figure 11 for the nanosecond Z-scan, the pure nonlinear refraction curve displays a peak−valley shape, indicating the self-defocusing nature of the nonlinear refraction of **1** for nanosecond laser pulses at 532 nm. By fitting this curve using eq 3, the on-axis phase change can be obtained. The

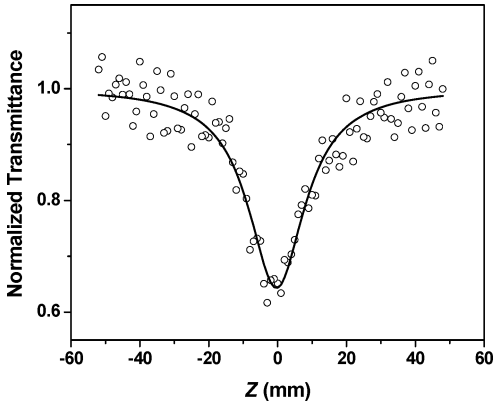

Figure 12. Open-aperture Z-scan of **1** using 27 ps laser pulses at 532 nm in a 2 mm cell. The incident energy of the laser beam is 2.9 μJ, and the concentration used is 2.1×10^{-3} mol/L.

TABLE 4: Ground-State and Excited-State Absorption Cross Sections of 1 at Different Wavelengths Measured by Picosecond Laser Pulses in a 2.1×10^{-3} mol/L Acetonitrile Solution

λ/nm	σ_0 (10^{-18}/cm^2)	σ_{ex} (10^{-18}/cm^2)	σ_{ex}/σ_0
500	4.9	8.3	1.7
532	1.6	10.5	6.6
550	0.69	16.9	24.5
570	0.30	48.0	160.0

nonlinear refractive index, n_2, is then calculated to be 7.57×10^{-17} (m^2/W), which corresponds to $\mathrm{Re}\chi^{(3)} = 5.77 \times 10^{-12}$ esu.

For nonlinear optical materials with cumulative nonlinearities, such as a system with reverse saturable absorption, the refractive index change is due to population redistribution. In such a case, the change in refractive index is better described by refractive cross section σ_r than by n_2. The σ_r is related to on-axis phase change $\Delta\Phi_0$ by[22]

$$\Delta\Phi_0 = \frac{\alpha}{2h\nu}\sigma_r F_0 L_{\mathrm{eff}} \tag{5}$$

where $F_0 = 2E/\pi\omega^2$. Using the $\Delta\Phi_0$ obtained by the fitting of the nonlinear refraction data by eqs 3 and 5, the σ_r is obtained to be 7.78×10^{-18} cm^2.

In addition to measuring the on-axis phase change ($\Delta\Phi_0$) and thus deducing the nonlinear refractive index n_2 and $\mathrm{Re}\chi^{(3)}$, Z-scan can be used to measure the transmission change induced by nonlinear absorption when no aperture is used in front of the detector, which is referred to as an open-aperture Z-scan. For **1**, a significant transmission drop is observed when the sample is moved closer to the focal plane, suggesting a strong reverse saturable absorption. For a Gaussian beam Z-scan, the excited-state absorption cross section can then be deduced from the fitting of the open aperture curve using eq 6[23]

$$T(z) = \ln\left(1 + \frac{q_0}{1+x^2}\right)\Big/\left(\frac{q_0}{1+x^2}\right) \tag{6}$$

where $q_0 = (\sigma_{ex}\alpha F_0(r=0)L_{\mathrm{eff}})/2\hbar\omega$, with $L_{\mathrm{eff}} = (1 - e^{-\alpha L})/\alpha$ and $F_0 = 2E/\pi\omega^2$.

This gives rise to $\sigma_{ex} = 1.93 \times 10^{-17}$ (cm^2) with $\sigma_{ex}/\sigma_0 = 12.1$, where σ_0 is determined by $\alpha = 10^{-3}\sigma_0 N_A C$.

For picosecond laser pulses, **1** exhibits nonlinear absorption from 500 to 570 nm, but no nonlinear refraction was observed in this spectral range. Fitting of the experimental curves by eq 6 results in the excited-state absorption cross section listed in Table 4. At longer wavelengths, the excited-state absorption cross section increases, while the ground-state absorption cross section decreases. As a result, the ratio of σ_{ex}/σ_0 has been increased to 160 at 570 nm, which is among the largest ratios reported in the literature.

Conclusion

The platinum(II) 4,6-diphenyl-2,2′-bipyridyl pentynyl complex **1** emits at room temperature and 77 K. It exhibits a broad and relatively strong triplet transient absorption from the near-UV to the near-IR spectral region, with a quantum yield of 0.51 for the triplet excited-state formation. Due to its reduced ground-state absorption at 532 nm, this complex exhibits strong RSA for both nanosecond and picosecond laser pulses. The RSA spans from 500 to 570 nm for picosecond laser pulses. The ratio of the excited-state absorption to the ground-state absorption cross section increases at longer wavelengths, with a ratio as high as 160.0 at 570 nm. In addition, it exhibits a self-defocusing effect for nanosecond laser pulses. Therefore, it is a promising nonlinear optical material for photonic devices that requires large and broadband third-order nonlinear optical responses.

Acknowledgment. This work is supported by the National Science Foundation (CAREER CHE-0449598) and Army Research Laboratory (W911NF-06-2-0032). We are grateful to Dr. Hongshan He for his help in obtaining the crystal structure.

Supporting Information Available: Crystal data (CIF file), crystal packing diagram, concentration-dependent emission spectra at room temperature and 77 K, temperature-dependent emission spectra, solvent-dependent emission spectra at room temperature, and optical density of transient absorption versus excitation energy for **1** at 585 nm. This material is available free of charge via the Internet at http://pubs.acs.org.

References and Notes

(1) (a) Dick, A. R.; Kampf, J. W.; Sanford, M. S. *Organometallics* **2005**, *24*, 482. (b) van der Boom, M. E.; Milstein, D. *Chem. Rev.* **2003**, *103*, 1759.

(2) (a) Lu, W.; Mi, B. X.; Chan, M. C. W.; Hui, Z.; Che, C. M.; Zhu, N.; Lee, S. T. *J. Am. Chem. Soc.* **2004**, *126*, 4958. (b) Yesin, H.; Donges, D.; Humbs, W.; Strasser, J.; Sitters, R.; Glasbeek, M. *Inorg. Chem.* **2002**, *41*, 4915. (c) Brooks, J.; Babayan, Y.; Lamansky, S.; Djurovich, P. I.; Tsyba, I.; Bau, R.; Thompson, M. E. *Inorg. Chem.* **2002**, *41*, 3055. (d) Shi, J. C.; Chao, H. Y.; Fu, W. F.; Peng, S. M.; Che, C. M. *J. Chem. Soc., Dalton Trans.* **2000**, *18*, 3128. (e) Chassot, L.; von Zelewsky, A.; Sandrini, D.; Maestri, M.; Balzani, V. *J. Am. Chem. Soc.* **1986**, *108*, 6084. (f) Maestri, M.; Sandrini, D.; Balzani, V.; Chassot, L.; Jolliet, P.; von Zelewsky, A. *Chem. Phys. Lett.* **1985**, *122*, 375. (g) Wong, W.-Y.; He, Z.; So, S.-K.; Tong, K.-L.; Lin, Z. *Organometallics* **2005**, *24*, 4079.

(3) (a) Wadas, T. J.; Chakraborty, S.; Lachicotte, R. J.; Wang, Q.-M.; Eisenberg, R. *Inorg. Chem.* **2005**, *44*, 2628. (b) Chakraborty, S.; Wadas, T. J.; Hester, H.; Flaschenreim, C.; Schmehl, R.; Eisenberg, R. *Inorg. Chem.* **2005**, *44*, 6865.

(4) (a) Yang, Q.-Z.; Wu, L.-Z.; Zhang, H.; Chen, B.; Wu, Z.-X.; Zhang, L.-P.; Tung, Z.-H. *Inorg. Chem.* **2004**, *43*, 5195. (b) Wu, L. Z.; Cheung, T. C.; Che, C. M.; Cheung, K. K.; Lam, M. H. W. *Chem. Commun.* **1998**, *10*, 1127. (c) Wong, K.-H.; Chan, M. C.-W.; Che, C. M. *Chem.—Eur. J.* **1999**, *5*, 2845. (d) Kui, S. C. F.; Chui, S. S.-Y.; Che, C.-M.; Zhu, N. *J. Am. Chem. Soc.* **2006**, *128*, 8297. (e) Wong, K. M.-C.; Tang, W.-S.; Lu, X.-X.; Zhu, N.; Yam, V. W.-W. *Inorg. Chem.* **2005**, *44*, 1492.

(5) McKay, T. J.; Staromlynska, J.; Davy, J. R.; Bolger, J. A. *J. Opt. Soc. Am. B* **2001**, *18*, 358.

(6) McEwan, K.; Lewis, K.; Yang, G.-Y.; Chng, L.-L.; Lee, Y.-W.; Lau, W.-P.; Lai, K.-S. *Adv. Funct. Mater.* **2003**, *13*, 863.

(7) Doyle, J. J.; Ballesteros, B.; de la Torre, G.; McGovern, D. A.; Kelly, J. M.; Torres, T.; Blau, W. J. *Chem. Phys. Lett.* **2006**, *428*, 307.

(8) Tutt, L. W.; Kost, A. *Nature* **1992**, *356*, 225.

(9) (a) Staromlynska, J.; McKay, T. J.; Bolger, J. A.; Davy, J. R. *J. Opt. Soc. Am. B* **1998**, *15*, 1731. (b) McKay, T. J.; Staromlynska, J.; Davy, J. R.; Bolger, J. A. *J. Opt. Soc. Am. B* **2001**, *18*, 358. (c) Zhou, G.-J.; Wong, W.-Y.; Cui, D.; Ye, C. *Chem. Mater.* **2005**, *17*, 5209. (d) Staromlynska, J.;

Chapple, P. B.; Davy, J. R.; McKay, T. J. *Proc. SPIE-Int. Soc. Opt. Eng.* **1994**, *2229*, 59.

(10) (a) Sun, W.; Wu, Z.-X.; Yang, Q.-Z.; Wu, L.-Z.; Tung, C.-H. *Appl. Phys. Lett* .**2003**, *82*, 850. (b) Guo, F.; Sun, W.; Liu, Y.; Schanze, K. *Inorg. Chem.* **2005**, *44*, 4055. (c) Sun, W.; Guo, F. *Chin. Opt. Lett.* **2005**, *S3*, S34. (d) Sun, W.; Zhu, H.; Barron, P. M. *Chem. Mater.* **2006**, *18*, 2602. (e) Guo, F.; Sun, W. *J. Phys. Chem. B* **2006**, *110*, 15029.

(11) (a) Appel, R.; Geisler, K.; Scholer, H. F. *Chem. Ber.* **1979**, *112*, 648. (b) Cheung, T.-C.; Cheung, K.-K.; Peng, S.-M.; Che, C. M. *J. Chem. Soc., Dalton Trans.* **1996**, 1645.

(12) Farrugia, L. J. *A Windows Program for Crystal Structure Analysis*; University of Glasgow: Glasgow, U.K., 1998.

(13) Sheldrick, G. M. *Programs for Crystal Structure Analysis*, release 97-2; University of Göttingen: Germany, 1997.

(14) Carmichael, I.; Hug, G. L. *J. Phys. Chem. Ref. Data* **1986**, *15*, 1.

(15) (a) Lu, W.; Mi, B. X.; Chan, M. C. W.; Hui, Z.; Che, C. M.; Zhu, N.; Lee, S. T. *J. Am. Chem. Soc.* **2004**, *126*, 4958. (b) Yang, Q.-Z.; Wu, L.-Z.; Wu, Z.-X.; Zhang, L.-P.; Tung, C.-H. *Inorg. Chem.* **2002**, *41*, 5653.

(16) (a) Kunkely, H.; Vogler, A. *J. Am. Chem. Soc.* **1990**, *112*, 5625. (b) Wan, K.-T.; Che, C.-M.; Cho, K.-C. *J. Chem. Soc., Dalton Trans.* **1991**, 1077.

(17) (a) Juris, A.; Balzani, V.; Barigelletti, F.; Campagna, S.; Belser, P.; Von Zelewsky, A. *Coord. Chem. Rev.* **1988**, *84*, 85. (b) Cummings, S. D.; Eisenberg, R. *J. Am. Chem. Soc.* **1996**, *118*, 1949. (c) Polo, A. S.; Itokazu, M. K.; Frin, K. M.; Patrocinio, A. O. D.; Iha, N. Y. M. *Coord. Chem. Rev.* **2006**, *250*, 1669. (d) Lai, S.-W.; Chan, M. C. W.; Cheung, K.-K.; Che, C.-M. *Inorg. Chem.* **1999**, *38*, 4262.

(18) Lu, W.; Chan, M. C. W.; Zhu, N.; Che, C.-M.; Li, C.; Hui, Z. *J. Am. Chem. Soc.* **2004**, *126*, 7639.

(19) Van Houten, J.; Watts, R. J. *J. Am. Chem. Soc.* **1975**, *97*, 4853.

(20) Sheik-Bahae, M.; Said, A. A.; Wei, T.-H.; Hagen, D. J.; Stryland, E. W. V. *IEEE J. Quantum Electron.* **1990**, *26*, 760.

(21) Butcher, P. N.; Cotter, D. *The Elements of Nonlinear Optics*; Cambridge University Press: Cambridge, U.K., 1993.

(22) Stryland, E. W. V.; Sheikbahae, M.; Said, A. A.; Hagan, D. *Proc. SPIE-Int. Soc. Opt. Eng.* **1993**, *1852*, 135.

(23) Wood, J. L.; Miller, M. J.; Mott, A. G. *Opt. Lett.* **1995**, *20*, 973.